

1 **Electronic supplementary information (ESI)**
2 **Plasmonic Enhancement of Photothermal Conversion in Hydrogels**
3 **using Gold Nanorods**

4 Mai S. Rashwan¹, Md. Masud Alam¹, Seyed Hassan Jaber², Abdel-Aziz Al-Sheikh¹, Anna
5 Christina S. Samia¹, Harihara Baskaran^{2*}, and Clemens Burda^{1*}

6 ¹ Department of Chemistry, Case Western Reserve University, Cleveland, OH, USA

7 ² Department of Chemical & Biomolecular Engineering, Case Western Reserve University,
8 Cleveland, OH, USA

9 * Corresponding authors: Harihara.Baskaran@case.edu, burda@case.edu

10	1. Instrumentation, Laser heating, and Thermal Conductivity Details.....	S2
11	2. Au NSs and Au NRs Characterization: Size Distribution and Zeta Potential.....	S5
12	3. Photothermal Heating of Au NS/hydrogels and Au NR/hydrogels using 785 nm and 808	
13	nm Laser Excitation.....	S6
14	3.1 Using 785 nm Laser Excitation.....	S7
15	3.2 Using 808 nm Laser Excitation.....	S9
16	4. Comparative Analysis of Experimental and Simulated Photothermal Energy Transfer	S11
17	4.1 Using 785 nm Laser Excitation.....	S11
18	4.2 Using 808 nm Laser Excitation.....	S12

19

20

21

22

23 **1. Instrumentation, Laser heating, and Thermal Conductivity Details**

24

25 **1.1. Characterization of Nanoparticles**

26

27 **1.1.1. UV-Vis Spectroscopy.** Absorbance spectra of Au NS dispersions, Au NR solutions, and
28 hydrogels were recorded using a UV-Vis-NIR spectrophotometer (Varian Cary 50). The
29 scans were performed at a rate of 600 nm/min over a wavelength range of 200-1000 nm
30 for Au NSs and 400-1100 nm for Au NRs. The measurements at 785 nm and 808 nm were
31 emphasized, as these wavelengths correspond to the laser wavelengths used for sample
32 heating.

33 **1.1.2. Transmission Electron Microscopy (TEM).** TEM was employed to characterize the
34 morphology of Au NSs and Au NRs. For sample preparation, 5 μ L of a dilute nanoparticle
35 suspension was deposited onto a 400 mesh Formvar-coated copper grid and allowed air-
36 dry at room temperature to ensure gradual evaporation of the solvent. Imaging was
37 performed using a FEI Tecnai G2 Spirit BioTWIN transmission electron microscope (FEI
38 Company, Hillsboro, OR), operated at an accelerating voltage of 120 kV. The particle size
39 distribution was determined by measuring the dimensions of 200 individual nanoparticles
40 and nanorods for each sample, and the resulting data were analyzed
41 using ImageJ software.

42 **1.1.3. Dynamic Light Scattering (DLS):** DLS and zeta potential analysis were conducted to
43 assess the Au NSs size distribution and surface charge in deionized water. Using the
44 Malvern Zeta Sizer Nano ZS, which employs a 633 nm laser in a backscattering
45 configuration (at 173°), measurements of particle size and zeta potential were taken, with
46 the results averaged over 10 scans to ensure reliability and accuracy.

47 **1.1.4. Atomic Absorption Spectroscopy (AAS):** Au-atom concentration was measured using
48 a Varian 240FS AA Atomic Absorption Spectrophotometer, a fast sequential instrument
49 designed for precise elemental analysis. It utilizes a flame atomizer to reduce gold ions
50 (Au^{3+}) to neutral atoms for detection. A gold-specific hollow cathode lamp (HCL) emitting
51 light at 242.8 nm serves as the excitation source, with absorbance measurements directly
52 correlating to the analyte concentration. The instrument enables accurate quantification of
53 gold by comparing sample absorbance to a calibration curve generated from standard
54 solutions.

55 **1.2. Laser Heating Set-up**

56
57 **1.2.1. Laser Excitation.** Two laser beams were used in the heating experiments, a PGL-H-785
58 nm 1 W laser, delivering an irradiance of $6.25 \times 10^3 \text{ W/m}^2$ and an MDL-III-808 nm 2W
59 laser, delivering an irradiance of $1.25 \times 10^5 \text{ W/m}^2$. The PCE was compared using both laser
60 sources. The 3D-printed container housing the Au NS and Au NR hydrogels was positioned
61 directly beneath the laser beam. To monitor temperature variations, eight thermocouples
62 were inserted through holes in the container's lid. These thermocouples calibrated using
63 standard ice point ($0 \text{ }^\circ\text{C}$) and boiling point ($100 \text{ }^\circ\text{C}$) methods, were then connected to a
64 digital thermometer and arranged approximately 3 mm apart along a 40 mm length inside
65 the container in a zigzag pattern. Temperature data were autonomously recorded at one-
66 minute intervals over a 15-minute period using monitoring software. This method, as
67 described in our previous publication,^{1,2} ensured precise tracking of temperature
68 fluctuations within the Au NP-hydrogel samples throughout the experiment. Each sample
69 was exposed to laser irradiation for 15 minutes, with temperature changes monitored at
70 eight spatially distributed locations. The first thermocouple (T_1) was placed at the laser

71 heating spot, and subsequent thermocouples (T_2 to T_8) were positioned at 5 mm intervals
72 from T_1 , with T_8 being the farthest from the heating spot. The temperature change (ΔT) at
73 each position was calculated as the difference between the recorded temperature after
74 irradiation every minute and the initial temperature prior to laser exposure, which served
75 as the control. This configuration adhered to our established setup for temperature
76 distribution measurements.

77 1.2.2. 3D-Printing

78 The design and fabrication of the box and cover were carried out using SolidWorks 3D
79 CAD Design software, followed by printing with a Formlabs Form 2 SLA 3D printer. After
80 the printing process, the components were thoroughly cleaned with isopropanol using a
81 Form Wash apparatus to remove residual printing material. The final curing step was
82 performed in a Form Cure unit, ensuring optimal hardness and durability of the printed
83 components for the intended experimental setup. The 3D-print file for the experimental
84 container is available upon request to help others reproduce the work and advance research.

85 1.3. Thermal Conductivity Measurements

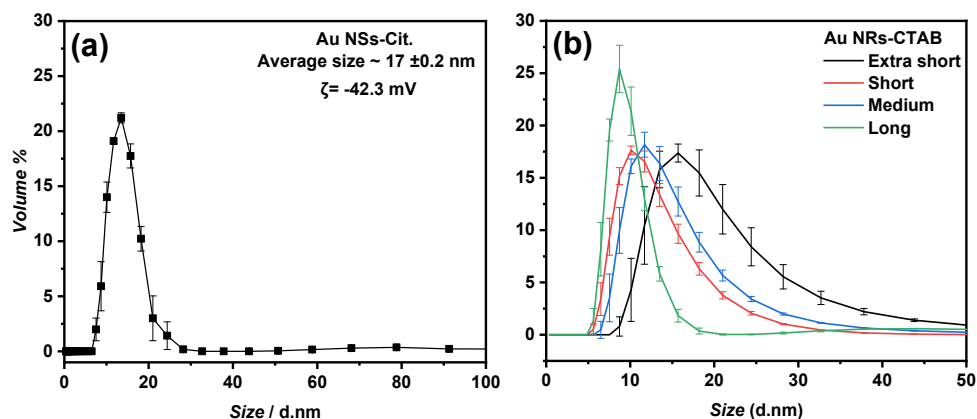
86 Thermal Conductivity (TC) of the samples was measured using the TEMPOS controller
87 TC analyzer (METER Group, Inc., USA) with a KS-3 stainless steel sensor needle (60 mm
88 in length, 1.3 mm in diameter). The measurement process involved 90-second cycles,
89 beginning with a 30-second equilibration phase, followed by alternating 30-second periods
90 of heating and cooling of the sensor needle. The temperature variations (ΔT) were used to
91 calculate the TC in units of $W/m \cdot K$, using the following equation:

$$92 \quad \kappa = \frac{q(\ln \frac{r_{20}}{r_{10}}(t_2) - \ln \frac{r_{20}}{r_{10}}(t_1))}{4\pi(\Delta T_2 - \Delta T_1)}$$

93 where q is the heat rate applied by the sensor, and ΔT_1 and ΔT_2 represent the temperature
94 differences at times t_1 and t_2 , respectively³⁻⁵.

95 **2. Au Nanosphere (NS) and Au NRs Characterization: Size and Zeta Potential**

96 The hydrodynamic diameter of the nanospheres was determined using dynamic light scattering
97 (DLS), revealing an average size of 17 ± 0.2 nm as presented by Fig. S1(a), indicative of a narrow
98 size distribution and high monodispersity. The sharp peak in the size distribution curve confirms
99 minimal aggregation and consistent particle synthesis. The zeta potential of the nanoparticles was
100 measured to be -42.3 mV, reflecting a strongly negative surface charge. This high zeta potential
101 value ensures excellent colloidal stability by promoting electrostatic repulsion between particles,
102 thereby preventing aggregation. The DLS measurements of the mean hydrodynamic diameters of
103 Au NRs, Fig. S1(b) are not intended to provide the actual particle size, as DLS is less accurate
104 than TEM for non-spherical particles. Instead, they demonstrate that the measured sizes follow the
105 same trend as the calculated nanoparticle volumes presented in Table 1 in the main manuscript.
106 These results confirm the successful synthesis of uniform and stable nanoparticles suitable for
107 further applications. In our previous work,² we employed SEM to image Au NS-embedded
108 hydrogels. Thus, a similar SEM study was not repeated in the current study. Nevertheless, we
109 ensured homogeneity in nanoparticle distribution through thorough mixing during gel formation
110 and optical extinction measurements, which showed reproducible spectra across independently
111 prepared samples.



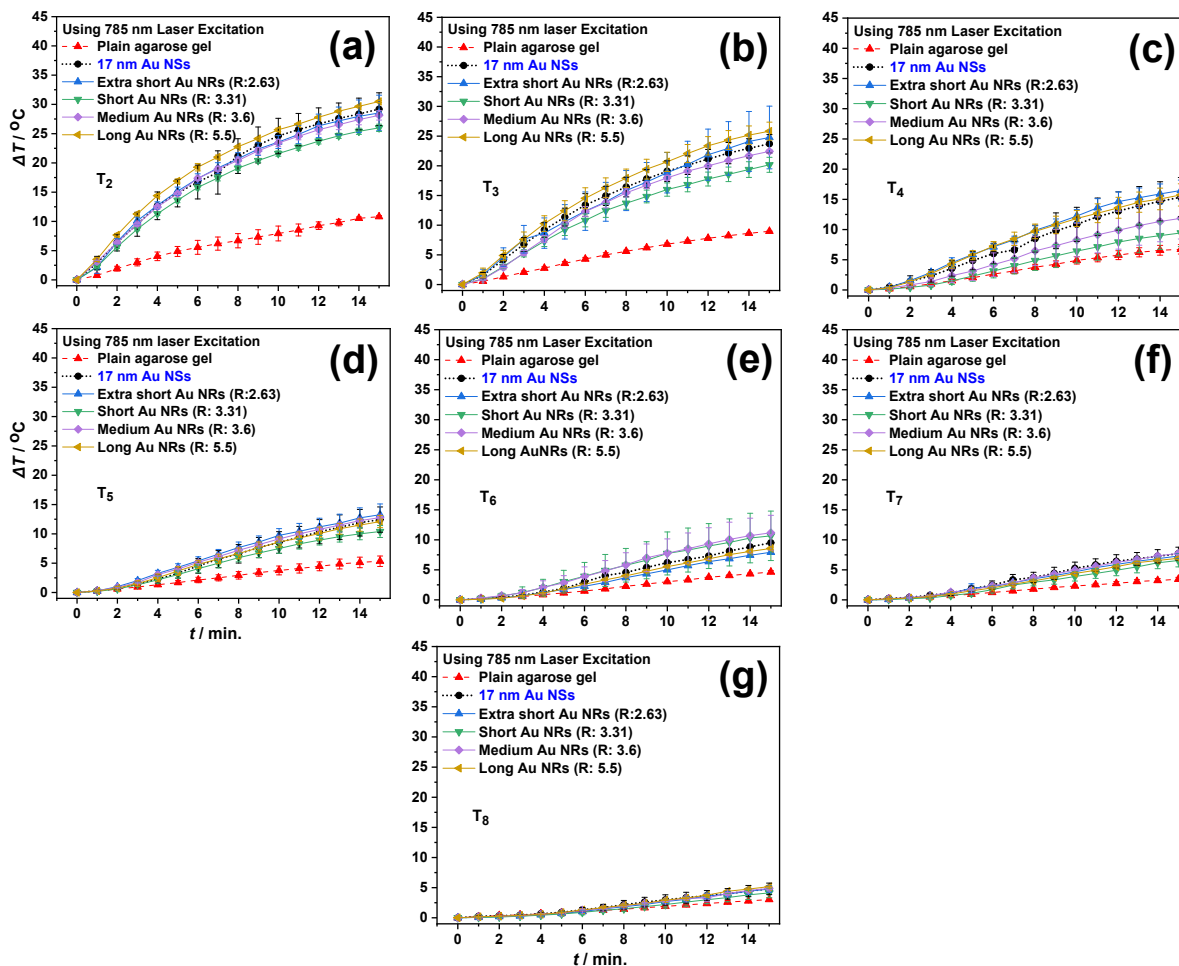
112

113 **Fig. S1.** DLS and Zeta potential measurements of (a) 17 nm spherical Au NSs and DLS
 114 measurements showing the mean hydrodynamic diameters of (b) Different sizes of Au NRs
 115 dispersed in DI water, showing the particle size distribution in volume% (N=3). Symbols represent
 116 the mean values, and vertical bars indicate the standard deviation.

117 **3. Photothermal Heating of Au NSs/hydrogel and Au NR/hydrogels using 785 nm and**
 118 **808 nm Laser Excitation**

119 The heat transfer profiles of Au NSs and Au NRs with varying ARs using 785 nm (Figure S2) and
 120 808 nm (Figure S4) laser irradiation are shown. In Figure S2, the temperature changes for the
 121 different nanoparticle shapes were comparable, with Au NSs and extra-short Au NRs (AR = 2.63)
 122 exhibiting slightly higher temperature increases relative to the plain agarose gel compared with
 123 other Au NR/hydrogels, across all monitored locations. In Figure S4, the highest temperature
 124 increases were observed for short Au NRs (AR = 3.31), with their LSPR peak at 820 nm, as well
 125 as Au NSs. These results indicate that despite the LSPR peak of the short Au NRs being slightly
 126 misaligned with the 808 nm wavelength, they still exhibit high photothermal heating efficiency,
 127 similar to Au NSs. Figures S3 and S5 show the temperature changes measured after 15 minutes
 128 of heating under 785 nm and 808 nm laser exposure for plain agarose, Au NSs/hydrogel, and Au
 129 NR/hydrogels, plotted against nanoparticle surface area, volume, and surface area-to-volume ratio
 130 (SA/V). The results demonstrate that these parameters do not significantly affect the photothermal

131 heating behavior under both laser wavelengths, consistent with the trends observed when aspect
 132 ratio is used as the x-axis in the main manuscript (Figs. 4 and 5).



133

134 **Fig. S2.** Temperature increase profiles as a function of time for Au NSs/hydrogel and different
 135 aspect ratio Au NR/hydrogels, heated using a 785 nm laser source at (A) T_2 : 5 mm and (B) T_3 : 7
 136 mm, (C) T_4 : 10 mm, (D) T_5 : 12 mm, (E) T_6 : 15 mm, (F) T_7 : 17 mm, (G) T_8 : 20 mm distance from
 137 the heating spot ($N=3$). Symbols represent the mean values, and vertical bars indicate the standard
 138 deviations. Laser exposure was applied at a radiation density of $2.08 \times 10^{-5} \text{ J/m}^3$, with an irradiance
 139 of $6.25 \times 10^3 \text{ W/m}^2$.

140

141

142

143

144

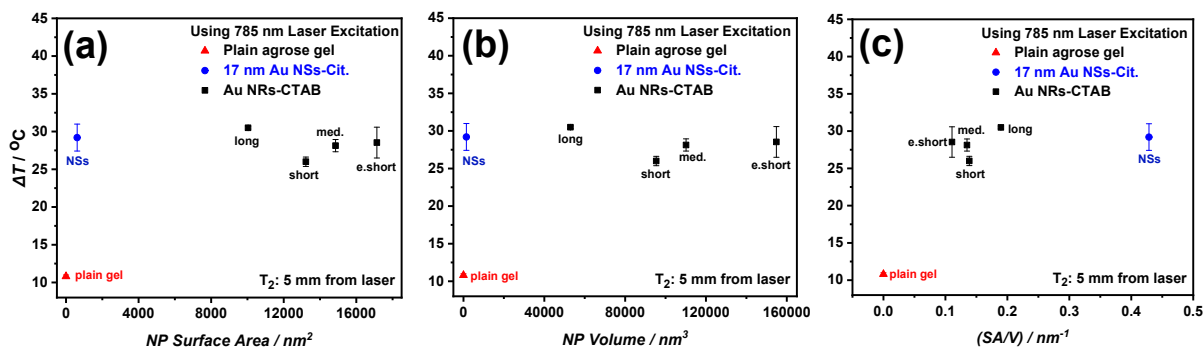
145

146

147 **Table S1** Temperature increase of Au NSs/hydrogel and Au NR/hydrogels under 785 nm laser
 148 irradiation at different distances (mm) from the heating spot

Au NP / Property	$\Delta T_2 / C$ (5 mm)	$\Delta T_3 / C$ (7 mm)	$\Delta T_4 / C$ (15 mm)	$\Delta T_5 / C$ (17 mm)	$\Delta T_6 / C$ (20 mm)	$\Delta T_7 / C$ (22 mm)	$\Delta T_8 / C$ (25 mm)
Plain agarose gel	10.2 ± 0.3	8.9 ± 0.0	6.5 ± 0.4	5.3 ± 0.9	4.6 ± 0.2	3.4 ± 0.3	3.0 ± 0.2
Au NSsj	29.2 ± 2.7	22.4 ± 0.3	15.3 ± 2.2	12.4 ± 2.2	9.5 ± 0.1	7.7 ± 1.1	4.8 ± 0.9
E. Short NRs (AR= 2.6)	28.5 ± 3.0	24.7 ± 5.2	16.4 ± 1.7	13.3 ± 1.8	7.9 ± 0.2	7.3 ± 0.5	4.7 ± 0.5
Short NRs (AR= 3.3)	26.0 ± 0.6	20.1 ± 1.3	9.4 ± 2.2	10.4 ± 1.0	10.6 ± 4.1	6.5 ± 1.0	4.1 ± 0.8
Med. NRs (AR= 3.6)	28.1 ± 0.8	25.8 ± 1.5	11.8 ± 3.4	12.7 ± 0.0	11.1 ± 2.9	7.7 ± 0.1	4.8 ± 0.2
Long NRs (AR= 5.5)	30.5 ± 0.1	23.7 ± 1.5	15.7 ± 1.8	12.1 ± 1.0	8.6 ± 0.2	6.9 ± 0.2	5.2 ± 0.0

149

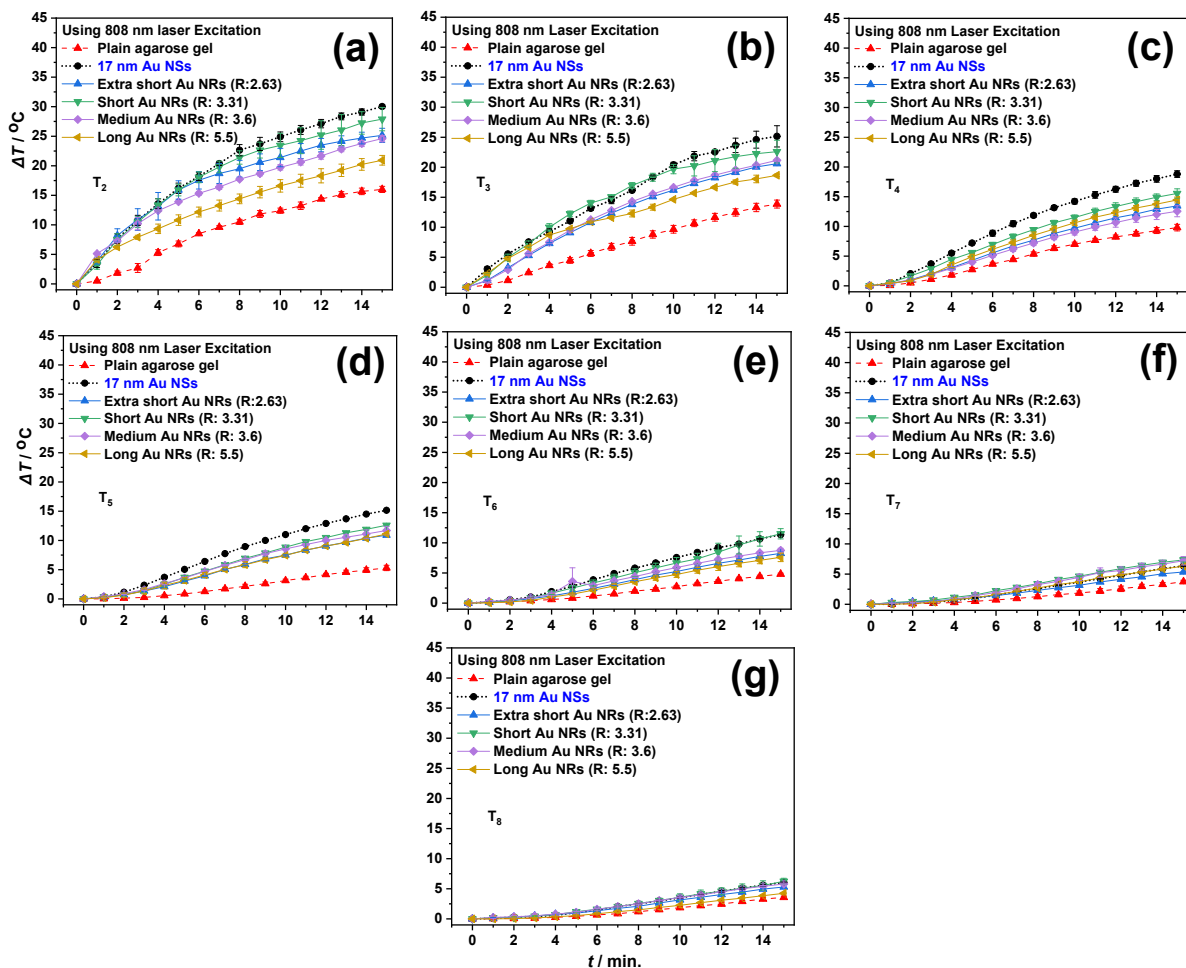


150

151 **Fig. S3** Temperature changes measured after 15 minutes heating under 785 nm laser exposure for
 152 plain agarose (red triangles), Au NSs/hydrogel (17 nm, blue circles), and Au NR/hydrogels with
 153 varying (a) NP surface area, (b) NP volume, and (c) NP surface area to volume ratio (SA/V) at 5
 154 mm distance (T_2) from the heating source. ($N=3$). The results indicate that surface area, volume,

155 and SA/V ratio of the nanoparticles do not significantly influence the photothermal heating
 156 profiles. Symbols represent mean values, and vertical bars indicate standard deviations.

157



158

159 **Fig. S4.** Temperature increase profiles as a function of time for Au NSs/hydrogel and different
 160 aspect ratio Au NR/hydrogels, heated using a 808 nm laser source at (A) T_2 : 5 mm and (B) T_3 : 7
 161 mm, (C) T_4 : 10 mm, (D) T_5 : 12 mm, (E) T_6 : 15 mm, (F) T_7 : 17 mm, (G) T_8 : 20 mm distance from
 162 the heating spot ($N=3$). Symbols represent the mean values, and vertical bars indicate the standard
 163 deviations. Laser exposure was applied at a radiation density of $4.17 \times 10^{-4} \text{ J/m}^3$, with an irradiance
 164 of $1.25 \times 10^5 \text{ W/m}^2$.

165

166

167

168

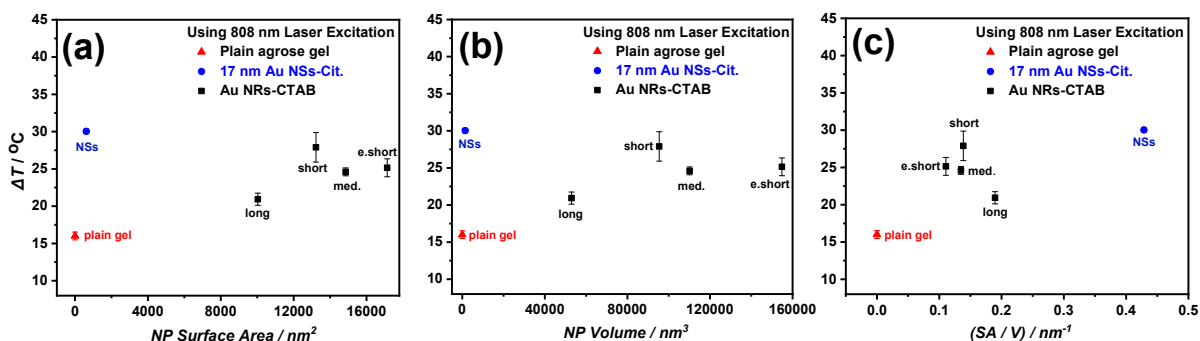
169

170

171 **Table S2** Temperature increase of Au NSs/hydrogel and Au NR/hydrogels under 808 nm laser
 172 irradiation at different distances (mm) from the heating spot

Au NP / Property	$\Delta T_2 / C$ (5 mm)	$\Delta T_3 / C$ (7 mm)	$\Delta T_4 / C$ (15 mm)	$\Delta T_5 / C$ (17 mm)	$\Delta T_6 / C$ (20 mm)	$\Delta T_7 / C$ (22 mm)	$\Delta T_8 / C$ (25 mm)
Plain agarose gel	16.0 ± 0.5	5.3 ± 0.6	9.8 ± 0.5	5.3 ± 0.4	4.8 ± 0.2	3.7 ± 0.2	3.0 ± 0.2
Au NSsj	30.0 ± 0.3	25.2 ± 1.7	18.8 ± 0.5	15.2 ± 0.1	11.3 ± 0.1	6.4 ± 0.1	6.0 ± 0.1
E. Short NRs (AR= 2.6)	25.1 ± 3.0	20.6 ± 0.1	13.4 ± 0.1	10.9 ± 0.0	8.2 ± 0.2	5.3 ± 0.1	5.3 ± 0.0
Short NRs (AR= 3.3)	27.9 ± 1.9	22.6 ± 1.9	15.5 ± 0.7	12.6 ± 0.1	11.5 ± 0.8	7.2 ± 0.7	6.3 ± 0.5
Med. NRs (AR= 3.6)	24.6 ± 0.5	21.2 ± 0.1	12.5 ± 0.9	11.7 ± 0.7	8.7 ± 0.3	7.4 ± 0.3	5.8 ± 0.1
Long NRs (AR= 5.5)	20.9 ± 0.8	18.6 ± 0.2	14.4 ± 0.5	11.1 ± 0.1	7.6 ± 0.7	6.3 ± 0.0	4.3 ± 0.1

173



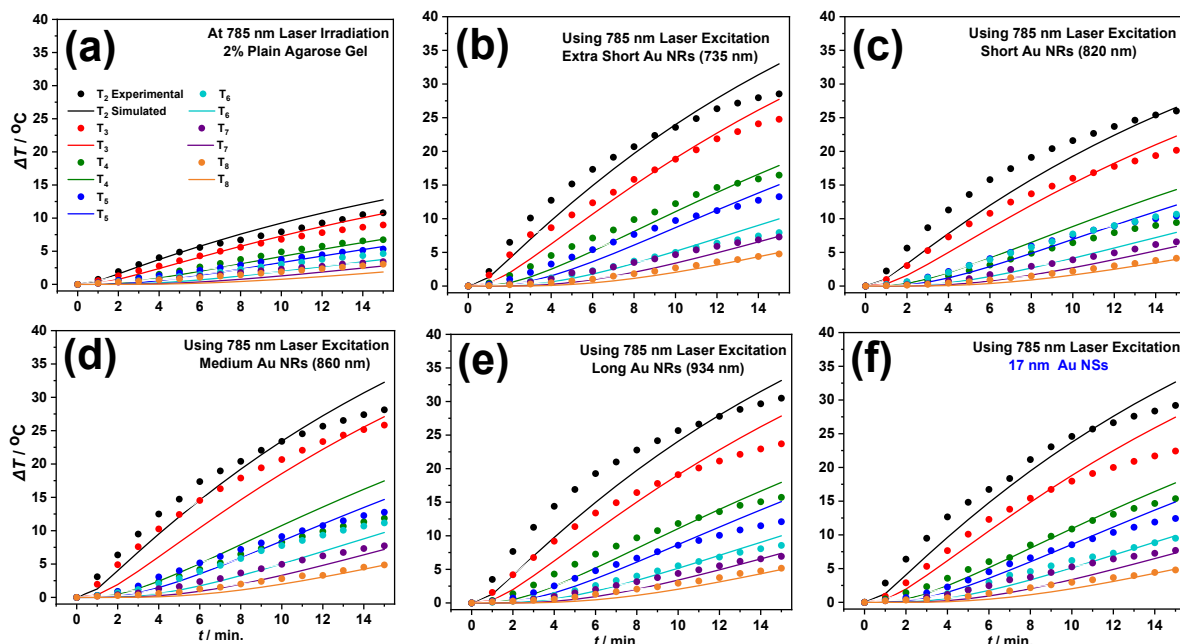
174

175 **Fig. S5** Temperature changes measured after 15 minutes heating under 808 nm laser exposure for
 176 plain agarose (red triangles), Au NSs/hydrogel (17 nm, blue circles), and Au NR/hydrogels with
 177 varying (a) NP surface area, (b) NP volume, and (c) NP surface area to volume ratio (SA/V) at 5
 178 mm distance (T_2) from the heating source. ($N=3$). The results indicate that surface area, volume,
 179 and SA/V ratio of the nanoparticles do not significantly influence the photothermal heating
 180 profiles. Symbols represent mean values, and vertical bars indicate standard deviations.

181

182 **4. Comparative Analysis of Experimental and Simulated Photothermal Energy**
183 **Transfer**

184 For each hydrogel run, we used a least-squares method to optimize the photothermal conversion
185 efficiency (η) by reducing the sum squared error between the experimental temperature data and
186 predictions from a transient 3D heat transfer model, which was developed and solved in COMSOL
187 Multiphysics 6.2 (Burlington, MA). The details of this are presented elsewhere ². Briefly, the
188 agarose gel was represented as a homogeneous 3D structure with the laser beam path modeled as
189 a solid square prism heat source. The sides of the gel were assumed to be insulated due to the
190 plastic enclosure surrounding the gel. We used temperature-dependent material properties of the
191 agarose gel ².



192

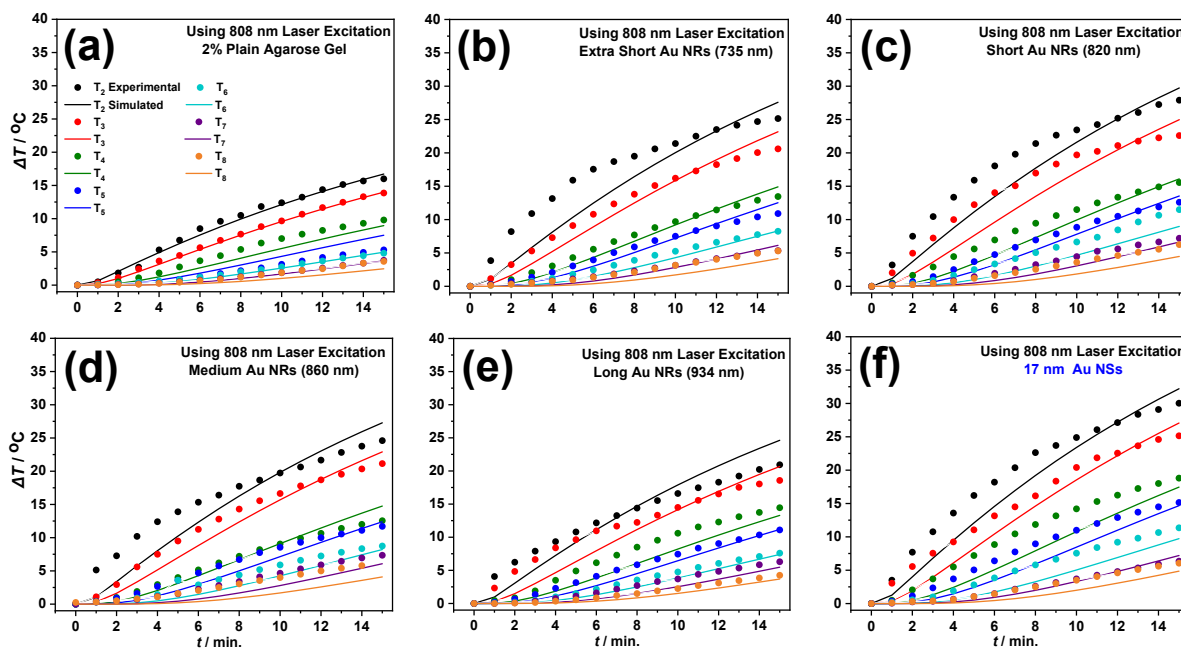
193 **Fig. S6.** Simulated (solid lines) and experimental (dots) temperature profiles as a function of time
194 upon heating with 785 nm laser source for various Au NSs/hydrogel and Au NR/hydrogels at
195 different distances from the heating spot for (a) Plain agarose gel, (b) Extra-short Au NRs, (c)
196 Short Au NRs, (d) Medium Au NRs, (e) Long Au NRs, and (f) 17 nm Au NSs. The close alignment
197 between the experimental and simulated results highlights the reliability and accuracy of the heat
198 conduction model.

199 **Table S3** Photothermal conversion efficiency (η , %) values of the Au NP/hydrogels upon
 200 irradiation with 785 nm laser.

201

Au NP / Property	Aspect Ratio (AR)	$\eta_{785 \text{ nm}}$ %
Plain agarose gel	0	28.02 ± 0.93
k Au NSs	1	71.31 ± 1.20
j Extra Short Au NRs	2.6	72.01 ± 1.07
Short Au NRs	3.3	58.02 ± 1.42
Medium Au NRs	3.6	70.42 ± 1.59
Long Au NRs	5.5	72.32 ± 1.10

202



203

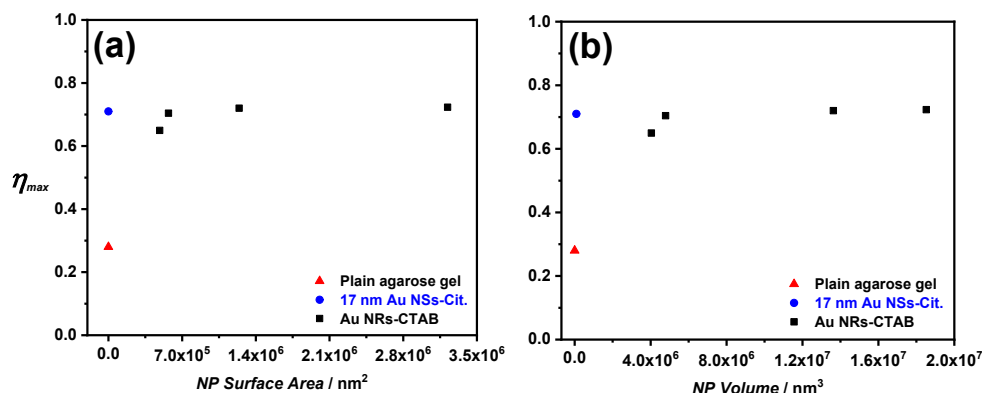
204 **Fig. S7.** Simulated (solid lines) and experimental (dots) temperature profiles as a function of time
 205 upon heating with 808 nm laser source for various Au NSs/hydrogel and Au NR/hydrogels at
 206 different distances from the heating spot for (a) Plain agarose gel, (b) Extra-short Au NRs, (c)
 207 Short Au NRs, (d) Medium Au NRs, (e) Long Au NRs, and (f) 17 nm Au NSs. The close alignment
 208 between the experimental and simulated results highlights the reliability and accuracy of the heat
 209 conduction model.

210 **Table S4** Photothermal conversion efficiency (η , %) values of the Au NP/hydrogels upon
 211 irradiation with 808 nm laser.

212

Au NP / Property	Aspect Ratio (AR)	$\eta_{808 \text{ nm}}$ %
Plain agarose gel k	0	36.65 \pm 0.76
Au NSs j	1	70.31 \pm 1.69
Extra Short Au NRs	2.6	60.30 \pm 1.16
Short Au NRs	3.3	64.95 \pm 1.60
Medium Au NRs	3.6	59.65 \pm 1.48
Long Au NRs	5.5	53.87 \pm 1.06

213



214

215 **Fig. S8** Maximum photothermal conversion efficiency (η_{max}) for plain agarose (red triangles), Au
 216 NSs/hydrogel (17 nm, blue circles), and Au NR/hydrogels with varying (a) NP surface area and
 217 (b) NP volume at 5 mm distance (T_2) from the heating source. These results confirm that neither
 218 surface is of the volume of the nanoparticle has an impact on η .

219

220

221

222

223

224

225

226 **References:**

- 227 1. M. S. Rashwan, H. Baskaran, C. Burda. *Adv. Funct. Mater.* 2024, **34**, 2309440.
- 228 2. M. S. Rashwan, A. M. Al-Sheikh, H. Baskaran and C. Burda, Plasmonic Enhancement of
229 Photothermal Conversion Efficiency in Gold-Nanoparticle Hydrogels, *ChemNanoMat*, 2025,
230 e202400636.
- 231 3. R. S. Khedkar, N. Shrivastava, S. S. Sonawane, K. L. Wasewar. *ICHMT* 2016, **73**, 5461.
- 232 4. M. Chandrasekar, S. Suresh, A. Chandra Bose. *Exp. Therm. Fluid Sci.* 2010, **34**, 210216.
- 233 5. J. K. Horrocks, E. McLaughlin. *Proc. R. Soc. A.* 1963, **273**, 259.